SANDIA REPORT

SAND2013-7656
Unlimited Release
September 2013

A compact single-camera system for high-speed, simultaneous 3-D velocity and temperature measurements

Louise Lu, Volker Sick, Jonathan H. Frank

![Sandia National Laboratories logo] Sandia National Laboratories

A compact single-camera system for high-speed, simultaneous 3-D velocity and temperature measurements

Louise Lu[1], Volker Sick[1], Jonathan H. Frank[2]
[1]Department of Mechanical Engineering
University of Michigan
Ann Arbor, MI 48109-2133

[2]Reacting Flows Department
Sandia National Laboratories
P.O. Box 969, MS 9051
Livermore, California, 94551-0969

Abstract

The University of Michigan and Sandia National Laboratories collaborated on the initial development of a compact single-camera approach for simultaneously measuring 3-D gas-phase velocity and temperature fields at high frame rates. A compact diagnostic tool is desired to enable investigations of flows with limited optical access, such as near-wall flows in an internal combustion engine. These in-cylinder flows play a crucial role in improving engine performance. Thermographic phosphors were proposed as flow and temperature tracers to extend the capabilities of a novel, compact 3D velocimetry diagnostic to include high-speed thermometry. Ratiometric measurements were performed using two spectral bands of laser-induced phosphorescence emission from $BaMg_2Al_{10}O_{17}$:Eu (BAM) phosphors in a heated air flow to determine the optimal optical configuration for accurate temperature measurements. The originally planned multi-year research project ended prematurely after the first year due to the Sandia-sponsored student leaving the research group at the University of Michigan.

ACKNOWLEDGMENTS

CONTENTS

FIGURES

Figure 1: The SC3D – PTV optical configuration. Two off-center optical paths are imaged through a single lens to achieve two viewing angles. A "beam twister" mirror set-up rotates the images by 90° to fit efficiently on the camera chip [9].. 11

Figure 2: 100 instantaneous raw particle images taken over 100 ms were evaluated using the SC3D – PTV algorithm and a stereo – PIV algorithm. The average 3C2D velocity field determined from 100 instantaneous SC3D – PTV measurements is shown on the left. The average 3C2D velocity field determined from 100 instantaneous stereo - PIV measurements is shown on the right.. 12

Figure 3: Spectral distribution of blackbody radiation for 300 – 800 K..................................... 17

Figure 4: (a) Normalized emission spectra of $BaMg_2Al_{10}O_{17}$:Eu (BAM) between 290 – 1150 K. The spectrum is centered around 440 nm but broadens toward the UV with an increase in temperature. A slight blueshift is also seen around 450 nm with increasing temperature; (b) BAM spectral intensity ratio calibration using 400 ± 20 nm and 456 ± 5 nm interference filters [21].. 18

Figure 5: Velocity response times of BAM particles (τ_p) after a step change in velocity are shown as a function of temperature for particle diameters of 1, 2, and 4 μm. Response times decrease with an increase in temperature. Smaller particles respond faster. 19

Figure 6: Thermal response times of BAM particles (t_{95}) initially at 300 K to a step change in gas temperature are shown as a function of gas temperature for particle diameters of 1, 2, and 4 μm. Response times decrease with an increase in the gas temperature. Smaller particles respond faster.. 20

Figure 7: The spectral ratio of baked BAM particles at 295 K and 805 K as a function of laser fluence. The error bars represent one standard deviation of the individual particle ratios. Ratios at both temperatures are independent of laser fluence. Ratios within one standard deviation at 295 K and 805 K overlap and therefore do not indicate a distinct difference in air temperature........ 23

Figure 8: The spectral ratio of unbaked BAM particles at 295 K and 805 K as a function of laser fluence. The error bars represent one standard deviation of the individual particle ratios. Ratios at

TABLES

ACRONYMS

3C2D: three-component, two-dimensional
3C3D: three-component, three-dimensional
BAM: barium magnesium aluminate doped with europium, $BaMg_2Al_{10}O_{17}$:Eu
FRS: filtered Rayleigh scattering
ICE: internal combustion engine
LIF: laser-induced phosphorescence
PIV: particle image velocimetry
PTV: particle tracking velocimetry
SC3D - PTV: single-camera, 3-D particle tracking velocimetry
SIDI: spark-ignited direct injection
TP: thermographic phosphor

1   INTRODUCTION

Technologies to improve fuel economy and pollutant formation in an internal combustion engine (ICE) are directly affected by mass and energy exchange processes within the cylinder boundary layers. Unfortunately, the fundamental physics of fluid flow and heat transfer within the boundary layers under transient high-pressure and high-temperature conditions are still not well understood. In-cylinder flows are highly turbulent and three-dimensional with characteristic flow structures that evolve on time scales of a millisecond or less [1]. Therefore, simultaneous, high-speed, 3-D measurements of spatially resolved velocity and temperature fields are necessary to characterize the structure and dynamics of turbulent, transient boundary layers within ICEs. These measurements are essential for developing and validating predictive fluid flow and heat transfer models of near-wall flows.

Several techniques for multi-dimensional, simultaneous velocity and temperature measurements have previously been demonstrated [2–4]. Each of these studies combined a velocity measurement technique, such as particle image velocimetry (PIV), with a thermometry technique, such as laser-induced fluorescence (LIF), filtered Rayleigh scattering (FRS), or thermographic phosphors (TP). Unfortunately, the experimental procedures described in these previous studies are not suitable for investigating near-wall flows in ICEs with limited optical access because they often require more than one camera, laser, or set of signal collection devices. However, Someya *et al.* [5] demonstrated a compact method of measuring simultaneous 2-D velocity and temperature measurements with TPs using a single camera and a single-pulsed UV laser. TPs exhibit temperature sensitive emission characteristics after excitation by a UV light source. Temperature may be inferred from the phosphorescence lifetime or from a ratio of two spectral bands [6–8]. Unlike the study performed by Omrane *et al.,* [4] the images of particle phosphorescence were used to infer velocity and temperature. This simplified approach may be modified to enable a single-camera diagnostic for simultaneous, 3-D gas-phase velocity and temperature measurements.

A single-camera approach for 3-D velocity measurements using a particle-tracking algorithm was recently developed at the University of Michigan [9] to enable flow investigations in regions of limited optical access. Thermographic phosphors were proposed as flow and temperature tracers to extend the capabilities of a novel, compact 3-D velocimetry diagnostic to include high-speed, 3-D thermometry. We proposed velocity measurements by tracking images of particle phosphorescence rather than the traditional Mie scattering to eliminate the need for an additional camera.

This report details the initial development of a single-camera technique for simultaneous, high-speed, 3-D gas-phase velocity and temperature measurements to facilitate time-resolved investigations of 3-D velocity and temperature distributions within near-wall flows. A description of the single-camera 3-D velocimetry diagnostic (SC3D – PTV) is provided in Section 2. Barium magnesium aluminate doped with europium ($BaMg_2Al_{10}O_{17}$:Eu), or BAM was identified as a suitable phosphor material for this work. The thermometry capabilities of thermographic phosphors, phosphor selection process for ICE applications, and particle flow and temperature tracing capabilities of BAM are discussed in Section 3. Sufficient phosphorescence signal strength is paramount for the success of this tool. The phosphorescence intensity of most

TPs decreases with an increase in temperature [8]. Furthermore, the signal strength is also sensitive to the excitation energy. TPs for gas-phase thermometry require higher laser fluence to achieve adequate signal compared to TPs for surface thermometry. However, high laser fluences may heat the TPs and cause a systematic error in the temperature measurement. Previous studies reported that laser fluences up to 1.5 J/cm^2 did not impact the spectral ratio for BAM at room temperature [10,11]. Therefore, spectral ratio measurements on BAM particles were performed in a heated air flow at 295 K and 805 K and laser fluences from 0.3 – 1.75 J/cm^2 to evaluate the phosphorescence signal strength as a function of temperature and laser fluence for accurate temperature measurements using non-intensified CCD cameras (Section 4). Finally, suggestions for future work are provided in Section 5.

2   SINGLE CAMERA, 3-D PARTICLE TRACKING VELOCIMETRY (SC3D - PTV)

This section provides an overview of the foundational principles and performance of the single - camera 3D velocimetry measurement technique, previously developed at the University of Michigan [9]. The single-camera, 3-D particle tracking velocimetry (SC3D – PTV) technique is a compact diagnostic tool recently developed for performing three-component volumetric velocity (3C3D) measurements in a limited measurement volume. Other 3C3D velocity measurement techniques, such as holographic PIV, defocusing PIV, fast-scanning PIV, and tomographic PIV [12–15], have limited spatial resolution, limited temporal resolution, or are not well-suited for flows in regions of limited optical access. The SC3D – PTV technique was developed to investigate the highly 3D nature of engine flows that have characteristic structures with millimeter length scales and evolve on time scales of a millisecond or less. Furthermore, the SC3D – PTV technique is designed for studying flows in regions with minimal optical access.

The SC3D-PTV technique only requires two points of optical access to image the flow and to illuminate the measurement volume with a light source propagating in the object plane. Two viewpoints of the same object are simultaneously imaged without perspective distortion using an optic that consists of one main lens and two off-center apertures each containing a smaller lens. A "beam twister" mirror set-up is used to focus and to rotate the simultaneously acquired images by 90° to fit efficiently onto a single camera chip. A schematic of the SC3D – PTV optical configuration is shown in Figure 1.
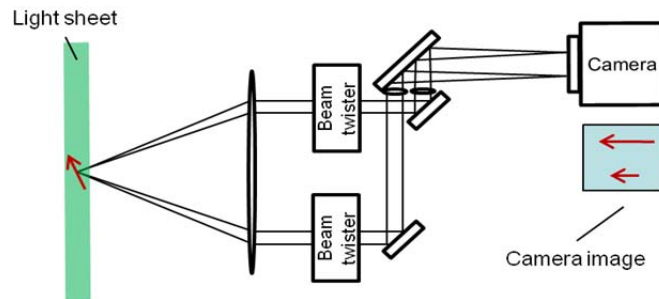
Figure 1: The SC3D – PTV optical configuration. Two off-center optical paths are imaged through a single lens to achieve two viewing angles. A "beam twister" mirror set-up rotates the images by 90° to fit efficiently on the camera chip [9]**.**

A single 3C3D velocity vector field is determined from a set of four images, or two pairs of successively captured images. Each pair of images consists of one image from each of the two simultaneously acquired viewing angles. The particle-tracking velocimetry (PTV) algorithm consists of two matching procedures: particle matching of simultaneously acquired images to determine instantaneous 3-D particle positions and particle matching of successive images to determine particle displacements. These matching procedures provide sufficient information to reconstruct a 3-D vector field without first recreating an instantaneous 3-D particle field. First, possible simultaneous particle matches are determined using epi-polar line considerations and potential successive particle matches are narrowed down to particles within a radius defined by an estimate of the maximum flow velocity. Next, an individual particle is identified from the potential simultaneous and successive matches and results in a set of four particle images (two simultaneous images and two successive images). Each valid vector in the vector field is the

result of a valid four-image set for a particle. A particle image may only be used in one four-image set. If a particle image is included in more than one four-image set, only the four-image set with the highest degree of similar features is retained. Particle image similarity is evaluated using seven features: 1) peak intensity 2) summed intensity 3) total number of pixels 4) width, as measured in pixels 5) height, as measured in pixels 6) maximum value of a cross-correlation between zero-padded raw particle images 7) maximum value of a normalized cross-correlation between zero-padded binarized particle images [9].

The SC3D – PTV technique was validated using stereoscopic – PIV (stereo – PIV). Stereo – PIV is an established technique that uses two simultaneously captured viewing angles to resolve three-component velocities in a plane (3C2D) [16]. A simple jet flow was imaged using the SC3D – PTV optic and then analyzed with both the SC3D – PTV algorithm and a stereo – PIV algorithm. The SC3D – PTV results were linearly interpolated onto a single – plane grid with the same grid – spacing as the stereo - PIV results to enable a comparison between both algorithms. The average 3C2D velocity field determined from 100 instantaneous SC3D – PTV measurements taken over a 100 ms time interval is shown on the left in Figure 2. The average 3C2D velocity field determined from 100 instantaneous stereo - PIV measurements taken over the same time interval is shown on the right in Figure 2. The two 3C2D velocity fields are qualitatively similar except at the edges where both algorithms suffer from particles traveling in and out of the measurement volume between camera exposures. Quantitatively, the SC3D – PTV results agreed with the stereo – PIV results within the uncertainty of stereo – PIV. The average velocity difference between the SC3D – PTV and stereo – PIV results was 3% with a maximum difference of 9%. More details on the experimental set-up and data processing for the validation may be found in [9].
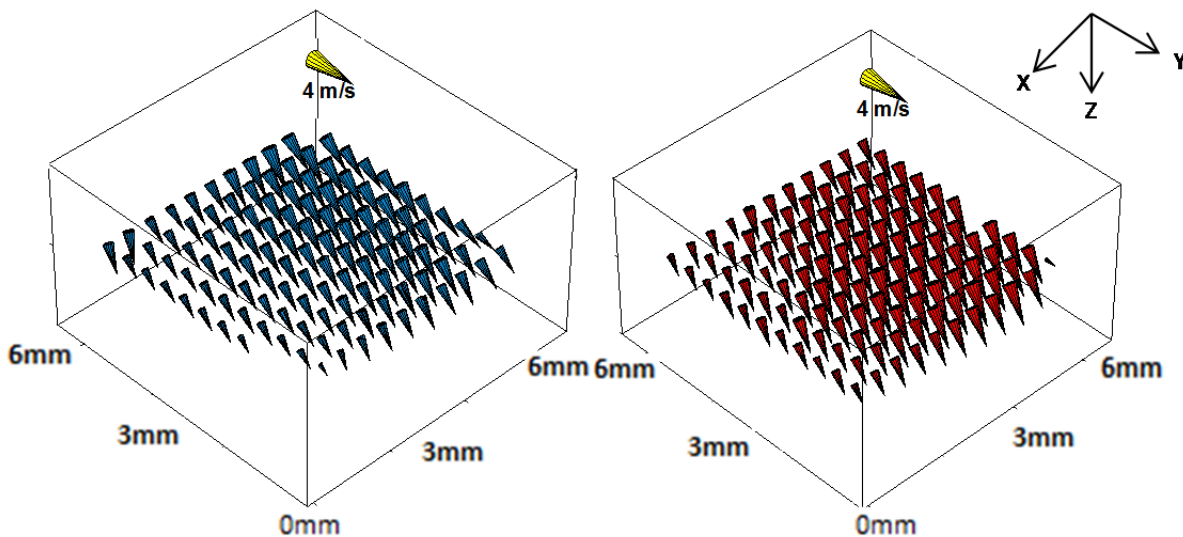
Figure 2: 100 instantaneous raw particle images taken over 100 ms were evaluated using the SC3D – PTV algorithm and a stereo – PIV algorithm. The average 3C2D velocity field determined from 100 instantaneous SC3D – PTV measurements is shown on the left. The average 3C2D velocity field determined from 100 instantaneous stereo - PIV measurements is shown on the right.

The capabilities of the SC3D – PTV technique may also extend to 3-D temperature measurements with the addition of thermographic phosphors particles. These particles could be used as flow and temperature tracers to enable simultaneous 3-D velocity and temperature measurement. Furthermore, the temperature distribution of simultaneous and successive image pairs could be used as an additional criterion for identifying valid four-image sets of each particle. The temperature sensitive emission characteristics of thermographic phosphors are described in the next section.

3   THERMOGRAPHIC PHOSPHORS

Thermographic phosphors are ceramic hosts doped with rare-earth ions that exhibit temperature sensitive emission characteristics after excitation by a pulsed light source (typically a UV source). The phosphorescence emissions of some TPs are significantly less sensitive to pressure and gas composition changes than other techniques, such as LIF. Temperature can be inferred by several methods using thermographic phosphors [7] but the lifetime of the phosphorescence decay or the ratio of two spectrally separated emission bands have emerged as the most popular methods [17].

The phosphorescence lifetime (τ) of most TPs is temperature dependent and emission intensities decay exponentially with time. For the simplest case, the phosphorescence decay may be modeled by a single exponential function:

$$I(t) = I_0 \exp(-t/\tau) \qquad \text{(Eq. 1)}$$

where $I(t)$ is the time-dependent intensity of the phosphorescence emission and I_0 is the initial intensity. The lifetime is defined as the time it takes for the intensity to reach $1/e$ of the initial intensity [6–8]. For TPs with phosphorescence lifetimes that do not follow a single exponential decay, expanded models may be used to assess and determine multiple lifetimes. A nonlinear fitting procedure is applied to fit the data to model and ultimately determine τ as a function of temperature. The lifetime approach is generally preferred over the spectral ratio method because it has a higher accuracy, precision, and temperature sensitivity [6–8,17–19]. However, the lifetime approach requires a minimum detection time span to resolve the phosphorescence decay and can be a limitation for high-speed measurements.

Unlike the lifetime approach, the spectral ratio method is based on temperature sensitive features of the phosphorescence emission spectrum. The temperature is determined from the ratio of two spectrally separated emission bands. If the distribution of electrons in the upper state is in thermal equilibrium, the phosphorescence signal from a transition associated with energy state i is given by the following expression:

$$S_i = C_i T_e \tau_i I_{laser} \exp\left(-\frac{E_i}{kT}\right), \qquad \text{(Eq. 2)}$$

where the parameters include detector efficiency (C_i), the camera exposure time (T_e), the optical filter transmission (τ_i), the laser pulse intensity (I_{laser}), the energy of the emitting state (E_i), temperature (T), and the Boltzmann constant (k). The total phosphorescence signal from one spectral band (S_λ) is the sum of all the phosphorescence emission peaks within the band. One advantage of taking the ratio of signal from two emission bands is that the resultant signal is independent of laser intensity:

$$R = \frac{S_{\lambda_1}}{S_{\lambda_2}} = \frac{\sum_i C_i \tau_i \exp\left(-\dfrac{E_i}{kT}\right)}{\sum_j C_j \tau_j \exp\left(-\dfrac{E_j}{kT}\right)}, \quad i \neq j$$

(Eq. 3)

where i denotes energy states the first spectral band (λ_1) and j denotes energy states the second spectral band (λ_2). Another advantage of the spectral ratio method is that short gate times are adequate for obtaining adequate signal. This enables measurements in environments with fast temperature fluctuations and suppresses background noise [8,20,21]. The disadvantage of this method is that it requires two independent and simultaneous measurements that must undergo an accurate background subtraction and image registration process before the ratio may be calculated. Despite this drawback, the spectral ratio method was used in this work to achieve high-speed measurements. In practice, the photophysics of many thermographic phosphors are not sufficiently understood to predict the temperature dependence of the signal ratio, R. As a result, the temperature dependence is determined using a calibration procedure involving the heating of the thermographic phosphor to known temperatures and measuring the signal ratios.

3.1 Phosphor selection

The test environments must be considered when choosing a suitable phosphor for the given application. First, the phosphor must exhibit adequate sensitivity in the temperature range of interest. Alternatively, a combination of phosphors may be used to span the desired temperature range. Other factors that impact the phosphor's emission characteristics must also be considered, such as pressure or gas composition effects. Next, the emission lifetimes over the temperature range must be sufficiently short to resolve the desired time scales. Phosphors with short emission lifetimes are also attractive because background radiation such as blackbody radiation and chemiluminescence can be suppressed using a short detector gate time. Phosphors that emit in the blue spectral region are less vulnerable to disturbances caused by black body radiation at high temperatures. Finally, the velocity and temperature tracing abilities of the phosphor must be assessed, and this is discussed in Section 3.2 [6–8,21].

The test environments considered were a heated jet and the motored spark-ignited direct-injection (SIDI) engine used in previous studies [22,23]. The temperature in these environments ranges from 300 – 800 K. The pressure in the motored SIDI engine spans 1 - 22 bar. The SIDI engine can operate up to 2000 rpm and corresponds to a repetition rate of 12 kHz for the laser and camera systems or a maximum exposure time of 83 µs to image every crank angle. Laser reflections off surfaces in the test environment will likely be the largest contributor to background intensity since this work will be performed in non-reacting flows. Additionally, any potential impact of blackbody radiation may be determined using Planck's distribution (Eq. 4) and is a function of wavelength (λ) at the blackbody temperature (T) [24]. Figure 3 shows the spectral distributions of blackbody radiation for the relevant temperature range

$$E = \frac{2\pi h c^2}{\lambda^5 \left[\exp\left(hc/\lambda kT\right) - 1\right]}$$

(Eq. 4)

16

E = Spectral emissive power [Wm^{-2}·µm^{-1}] h = Planck's constant [J·s]
λ = Wavelength of light [m] k = Boltzmann's constant [J/K]
T = Blackbody temperature [K] c = Speed of light [m/s]
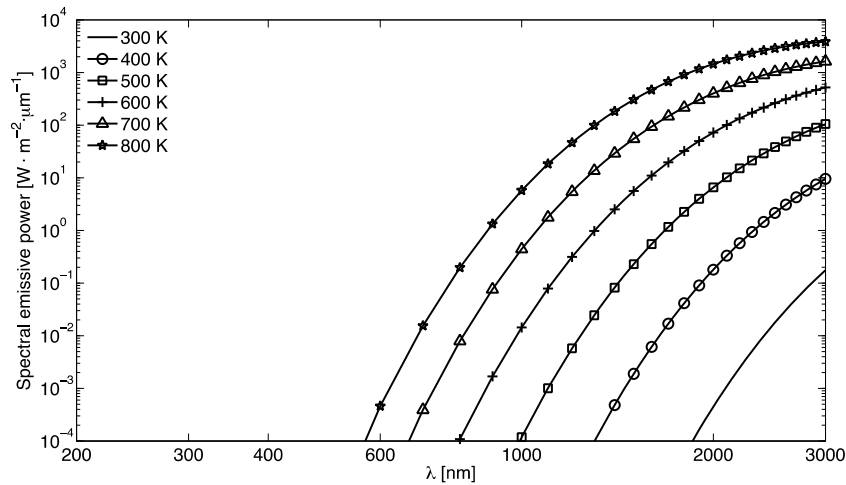

Figure 3: Spectral distribution of blackbody radiation for 300 – 800 K.

The emission characteristics of europium activated barium magnesium aluminate (BaMg$_2$Al$_{10}$O$_{17}$:Eu), or BAM, are suitable for the heated jet and motored SIDI engine. BAM is a stable phosphor with a broadband emission spectrum that peaks at 440nm when excited with UV light at 355 nm. The phosphor emits light for temperatures up to 1200 K and the lifetime decreases from 20 µs at room temperature to 10 ns at 1150 K. It has a melting point of 2190 K which makes it an attractive phosphor for combustion applications [8,21]. BAM emissions exhibit a slight redshift for high pressures, but this shift is negligible under 1 kbar [25]. The emission spectrum broadens toward the shorter wavelengths with increasing temperature, but the peak remains at 440 nm. A slight blueshift around 450 nm is also observed with increasing temperature (Figure 4a). Similar to most phosphors, the signal strength decreases with an increase in temperature but the simultaneous decrease in lifetimes enable short gate times for better background discrimination. A comparison Figs. 3 and 4a shows that the BAM phosphorescence emission wavelengths are well below those of the blackbody radiation. A temperature sensitive ratio can be achieved by detecting phosphorescence at 450 nm and at a wavelength that is on short-wavelength side of the emission peak. Figure 4b shows a calibration obtained by Särner *et al.* [21] using bandpass interference filters with center wavelengths at λ_c = 400 nm (FWHM = 40 nm) and λ_c = 456 (FWHM = 10 nm).

There are several reports regarding the use of BAM for temperature measurements greater than 800 K that lasted for an hour. Thermal degradation was observed for phosphor samples exposed to temperatures exceeding 800 K. The thermal degradation is attributed to the change in oxidation state of Eu^{2+} to Eu^{3+} and the migration of Eu^{2+} in the host lattice[26,27]. This leads to an irreversible decrease in phosphorescence intensity at room temperature and results in

17

inaccurate temperature measurements. However, residence times of particles in the present test environment are expected to be several orders of magnitude smaller than the time required for thermal degradation in BAM samples. Further work is required to determine the effect of short residence times on BAM phosphorescence.
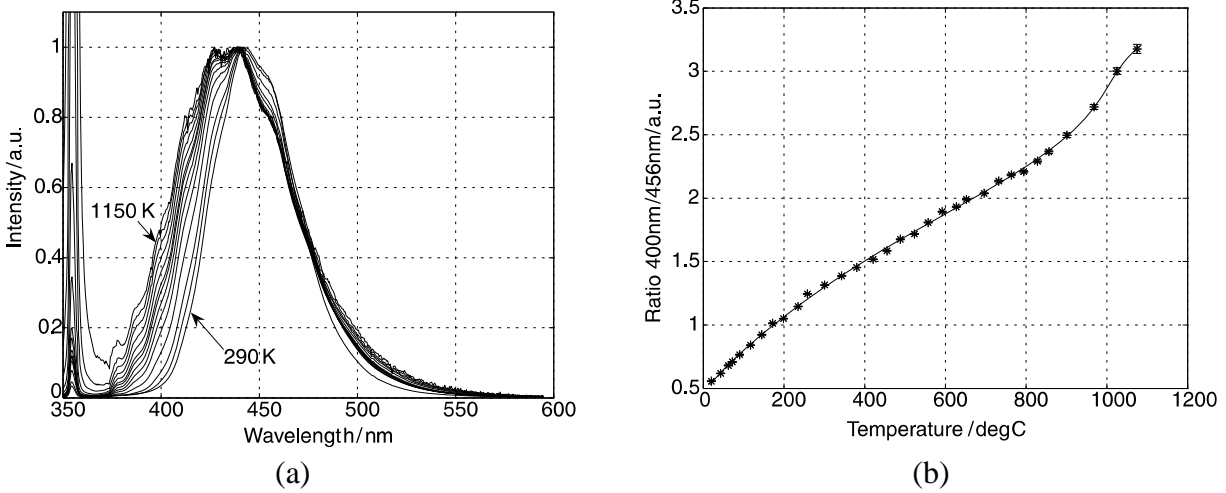

(a)   (b)

Figure 4: (a) Normalized emission spectra of BaMg$_2$Al$_{10}$O$_{17}$:Eu (BAM) between 290 – 1150 K. The spectrum peaks near 440 nm at room temperature but broadens toward the UV with an increase in temperature. A slight blueshift is also seen around 450 nm with increasing temperature; (b) BAM spectral intensity ratio calibration using λ_c = 400 nm (FWHM=40 nm) and λ_c = 456 nm (FWHM=10 nm) interference filters [21]

3.2 Velocity and temperature tracing capabilities

The accuracy of velocity and temperature measurements using TPs depends on the time required for the TP particles to respond to changes in the velocity and temperature of the fluid. Therefore, the particle velocity and thermal response times must be smaller than the flow time scales. Time scales in engine flows may be characterized by the engine time scale (τ_e), the turbulent turn over time scales (τ_t), and the resolved eddies turn-over time scales (τ_Δ) using the analysis from [22,28]. These time scales for the motored SIDI engine running at 2000 rpm are shown in Table 1. The grid spacing from Alharbi's [22] high resolution experiments of engine boundary layers were used in these estimates of τ_Δ.

τ_e [s]	τ_t [s]	τ_Δ [s]
1.5×10^{-2}	$5.0 \times 10^{-4} - 3.3 \times 10^{-3}$	$7.4 \times 10^{-5} - 1.5 \times 10^{-4}$

Table 1: Characteristic time scales for various flow structures in the engine: the engine time scale (τ_e), the turbulent turn over time scales (τ_t), and the resolved eddies turn-over time scales (τ_Δ) for the motored SIDI engine running at 2000 rpm.

When the density of the tracer particle (ρ_p) is much larger than the density of the surrounding fluid (ρ_f), as is the case for gas flows, the particle response to a step change in velocity may be characterized by a time constant:

18

$$\tau_p = \frac{\rho_p d_p^2}{18\mu_f}$$

(Eq. 5)

where d_p is the diameter of the particle and μ_f is the dynamic viscosity of the gas as determined by Sutherland's formula [29]. The particle's velocity response time is the time it takes for the particle to reach 95% of the flow velocity and occurs at $3\tau_p$. Particle velocity response times must be smaller than the time scales corresponding to the flow structures of interest. Particle response times for $d_p = 1$, 2, and 4 μm as a function of gas temperature are shown in Figure 5.
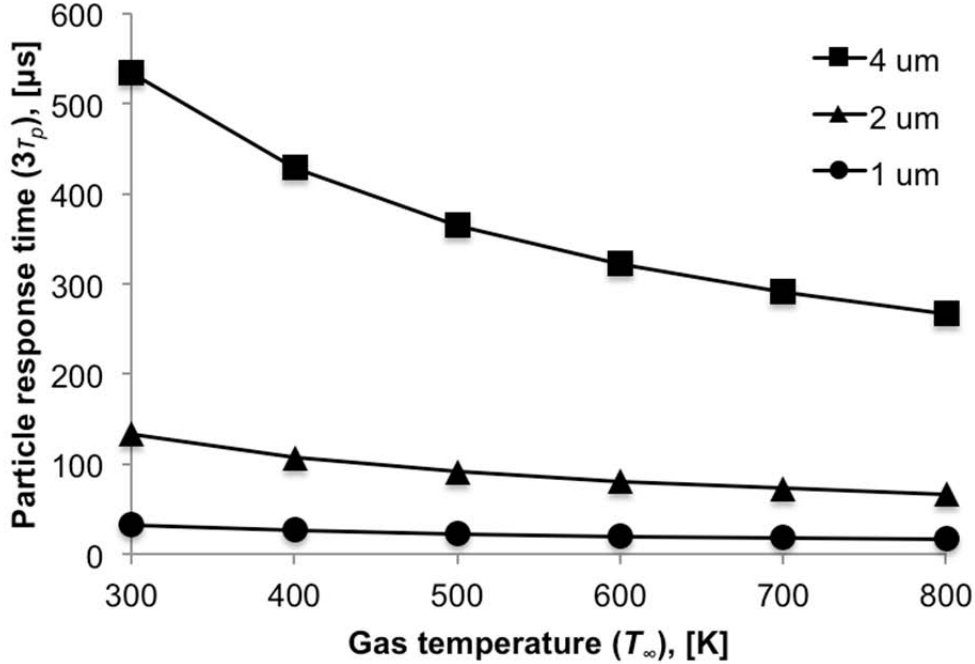

Figure 5: Velocity response times of BAM particles (τ_p) after a step change in velocity are shown as a function of temperature for particle diameters of 1, 2, and 4 μm. Response times decrease with an increase in temperature. Smaller particles respond faster.

BAM particles of $d_p = 1$ μm are ideal for accurately tracking the various engine flow structures corresponding to the time scales for an engine operating at 2000 rpm (Table 1). Unfortunately, the smallest BAM particles commercially available have a mean diameter of $d_p = 1.8$ μm. Therefore, only flows at lower engine speeds can be investigated while accurately resolving smaller flow structures when using these particles.

For an accurate temperature measurement based on the phosphorescence emission of the TP, the particle must be in thermal equilibrium with the surrounding gas. If the particles accurately follow the flow, the main modes of heat transfer to the particle are conduction and radiation. The particle's thermal response time was evaluated using Konopliv and Sparrow's analytical solutions for a 1-D, transient conduction heat transfer model [30] of a spherical particle at an initial temperature (T_{p0}) surrounded by an infinite gas with a uniform temperature (T_∞). The thermal properties of BAM are currently not well characterized and therefore thermal properties of YAG were used in the model [31]. The model assumes a uniform temperature for the particle since its thermal conductivity (k_p) is several orders of magnitude greater than the surrounding

19

gas. The model also assumes uniform gas thermal properties and constant particle thermal properties. The thermal response time (t_{95}) is the time it takes for the particle's temperature to reach 95% of its steady state value after a step change in the gas temperature. Figure 6 shows t_{95} as a function of T_∞ for d_p = 1, 2, and 4 μm with T_{p0} = 300 K.
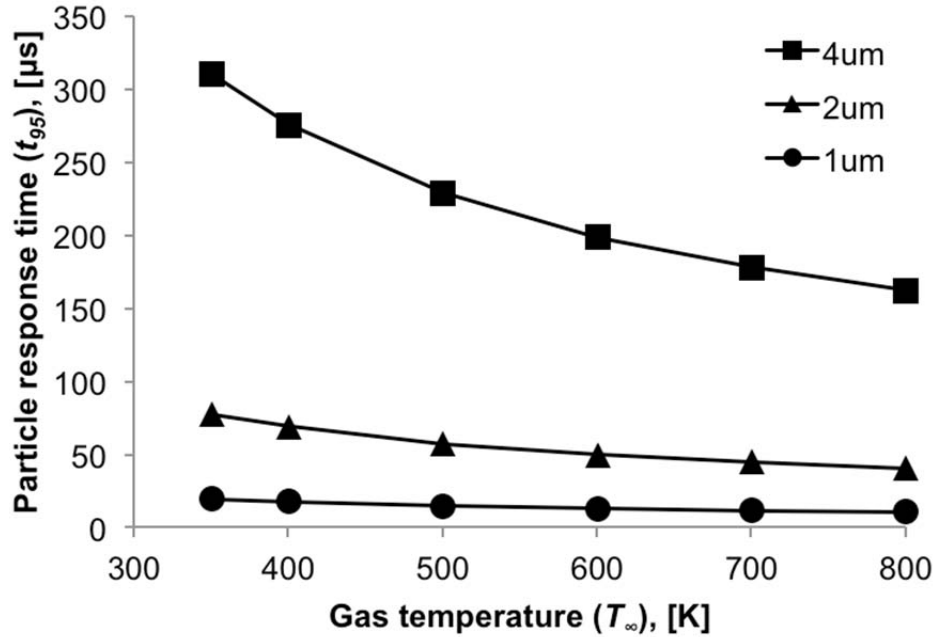

Figure 6: Thermal response times of BAM particles (t_{95}) initially at 300 K to a step change in gas temperature are shown as a function of gas temperature for particle diameters of 1, 2, and 4 μm. Response times decrease with an increase in the gas temperature. Smaller particles respond faster.

The decrease in t_{95} with increase in T_∞ is due to the increase in gas thermal diffusivity [11]. As expected, smaller particles equilibrate to the surroundings faster. Fond et al. [11] developed a numerical model to evaluate the effects of local temperature dependent gas thermal properties on particle thermal response time for a particle at T_{p0} = 300 K. The numerical model predicted that t_{95} increases for a cold particle in a hot environment because the gas thermal diffusivity in the vicinity of the particle is lower and hinders conductive heat transfer. Furthermore, Fond *et al.* [11] considered the case of a hot particle in cold surroundings and modeled the particle as a blackbody. Their results indicate that radiation heat loss contributes a small steady state error to the temperature, and the error increases with T_∞ or particle diameter but does not significantly affect t_{95}. Overall, BAM particle thermal response times are faster than their velocity response times. Therefore BAM particles are also suitable gas-phase temperature tracers.

4   HEATED JET EXPERIMENTS

Spectral ratio measurements on BAM particles (Phosphor Technology, 1.8 μm mean diameter) were performed in a heated air flow at 295 K and 805 K for a range of fluences from 0.3 – 1.75 J/cm^2.   The BAM phosphorescence signal decreases with an increase in temperature, as is the case for most TPs [21]. Measurements on BAM phosphors were evaluated at both ends of the relevant temperature range to determine the optimal configuration to achieve adequate signal strength for accurate temperature measurements. The signal strength is also sensitive to the excitation energy. TPs for gas-phase thermometry require higher laser fluence to achieve adequate signal compared to TPs for surface thermometry because of the sparse seeding density needed for undisturbed flow behavior and successful imaging conditions for particle tracking velocimetry. However, high laser fluences may heat the BAM particles and cause a systematic error in the temperature measurement. Previous studies have shown that laser fluences up to 1.5 J/cm^2 did not impact the spectral ratio for BAM at room temperature [10,11]. Although low laser fluence can be used, the weak signals my require the use of an image intensifier. However, non-intensified CCDs are preferable and are used in this study because intensified systems have a smaller dynamic range, spatially non-uniform gain, nonlinear responses, reduced spatial resolution, and higher noise levels [32,33].

4.1   Experimental set-up

A heated jet and a solid particle seeder for low flow rates were constructed for these studies. The jet set-up consisted of a heated laminar air flow (10.5 mm inner diameter) surrounded by a nitrogen coflow (43 mm diameter). The purpose of the coflow was to stabilize the heated jet. The central jet was constructed using a quartz tube. Heating was achieved through nichrome heating ribbon (H Cross) wrapped around the quartz glass tube and connected to a variable AC transformer. The heated tube assembly was thermally and electrically insulated from the rest of the set-up by two layers of flexible high-temperature ceramic insulation (Zircar Zirconia, Inc., ZYF - 100) and a ceramic shell. The temperature of the jet was monitored by a K-type thermocouple (Omega) placed 5 mm above the jet exit on the centerline. The thermocouple was translated horizontally across the jet using a micrometer stage. The flow rates for the central jet and coflow were adjusted to achieve a uniform temperature across the jet, which was verified using acetone LIF imaging. Flow rates through the central jet and the coflow were 8 slpm and 40 slpm, respectively, at 295 K and 3 slpm and 25 slpm, respectively, at 805 K.

Laser-induced phosphorescence was excited using a frequency tripled Nd:YAG laser (Surelite Continuum) producing 355 nm light at 10 Hz. The laser beam was reflected off several high-reflectivity mirrors (Lattice-Electro Optics) and passed through a half-wave plate (Lattice-Electro Optics), polarizer (Lattice-Electro Optics), and a cylindrical lens (f = 300 mm) before finally being directed over the centerline of the jet with another high-reflectivity mirror. The half-wave plate was rotated to vary the laser fluence and the cylindrical lens focused the laser beam into a narrow light sheet. The height and thickness of the light sheet were 1 cm and 0.05 cm, respectively.

Images of particle phosphorescence were collected at 10 Hz using two hardware-binned (2 x 2) 12-bit non-intensified CCD cameras (Cooke PCO Sensicam) placed on opposite sides of the heated jet. Camera 1 was fitted with a 50 mm f/1.2 Canon lens and a 400 ± 20 nm interference

filter (Andover). Camera 2 was fitted with a 50 mm f/1.4 Nikon lens and a 456 ± 5nm interference filter (Andover). Phosphorescence signal strengths through the 400 ± 20 nm filter were weaker than the signals through the 456 ± 5 nm filter. Therefore, the larger aperture lens was used with the 400 ± 20 nm filter to improve the signal collection efficiency. A 5 µs exposure time was used for both cameras.

Baked BAM particles were used for the first set of experiments to reduce the formation of particle agglomerates. The particles were baked at 473 K for 8 hours. 300 sparsely seeded images of particle phosphorescence were taken at 295 K and 805 K. At each temperature, the laser fluence was varied from 1 J/cm^2 to 1.75 J/cm^2 in 0.25 J/cm^2 increments. A low seeding density was necessary to distinguish individual particles during image post-processing. For each camera, background images were recorded with the laser sheet present but without particles. The same procedure was repeated to acquire sparsely seeded phosphorescence images of unbaked BAM particles at 295 K and 805 K. The laser fluence was varied from 0.3 to 0.9 J/cm^2 in 0.3 J/cm^2 increments for each temperature to evaluate a lower range of fluences that are similar to those used in Ref. [11]

4.2 Image Post-Processing and Data Analysis

Image post-processing was performed using the Matlab image toolbox. First, average background images for each laser fluence were subtracted from the particle phosphorescence images at the corresponding laser fluences. Then, the images were cropped to a region in the center of each detector to minimize vignetting effects. Alternatively, a flat-field correction can be performed using additional measurements. Next, image registration was performed by manually selecting approximately 30 particle image pairs from a set of simultaneously acquired images. The quality of the image registration was evaluated by performing a PIV analysis on particle image pairs after the image matching, and the resulting error of the particle positions was on the subpixel level. Therefore, the image registration aligned the simultaneously captured particle phosphorescence images with subpixel accuracy. Next, individual particles were identified in each image. A particle was defined as a group of three or more contiguous pixels with signals above 10 A/D counts. The particle size was defined as the number of pixels in the group. Each particle image from camera 1 was matched to the corresponding particle image in camera 2 if the location of the centroids of the matched particle images were within one pixel of each other. Next, the signals from each particle image were summed over the contiguous pixels, where S_1 and S_2 are the integrated signals from cameras 1 and 2, respectively. Finally, the spectral ratio of each particle was determined from the ratio of S_1 to S_2. The average spectral ratio for each temperature and laser fluence combination was determined by averaging the spectral ratio from many individual particles. The standard deviation of the average ratio was also determined.

4.3 Results and Discussion

The dependence of the average spectral ratios on laser fluence for baked BAM particles seeded into heated air flows at 295 K and 805 K are shown in Figure 7. The error bars in the plot indicate one standard deviation for the spectral ratios that were measured for all particles at each condition. At each temperature, the variation in the average spectral ratios ($R_{295\ K}$ and $R_{805\ K}$, respectively) for laser fluences between 1 J/cm^2 and 1.75 J/cm^2 is within one standard deviation of the corresponding signal ratios. Similar insensitivity of signal ratios to laser fluence were reported in previous studies by Lindén *et al.* [10] and Fond *et al.* [11]. At each laser fluence, the

average value of $R_{805\,K}$ is larger than that of $R_{295\,K}$. However, the temperature dependence of R is significantly smaller than that shown in Fig. 4b. Previous gas-phase thermometry studies using BAM particles [11,34], indicate that $R_{805\,K}$ is approximately twice as large as $R_{295\,K}$. In Fig. 7, the average values of $R_{805\,K}$ remain within one standard deviation of the average values of $R_{295\,K}$, indicating the need to average over many particles in order to resolve a temperature difference. A potential cause for this lack of temperature sensitivity is the baking of the BAM particles prior to using them in the experiment. Significant degradation in the phosphorescence emission due to oxidation has been reported for BAM phosphors baked at temperatures greater than 673 K for 2.5 hours [26]. However, the time scales at which oxidation occurs has not been determined. Therefore, a standard procedure for baking the BAM phosphors at temperatures lower than 673 K to reduce particle agglomeration has not yet been developed.
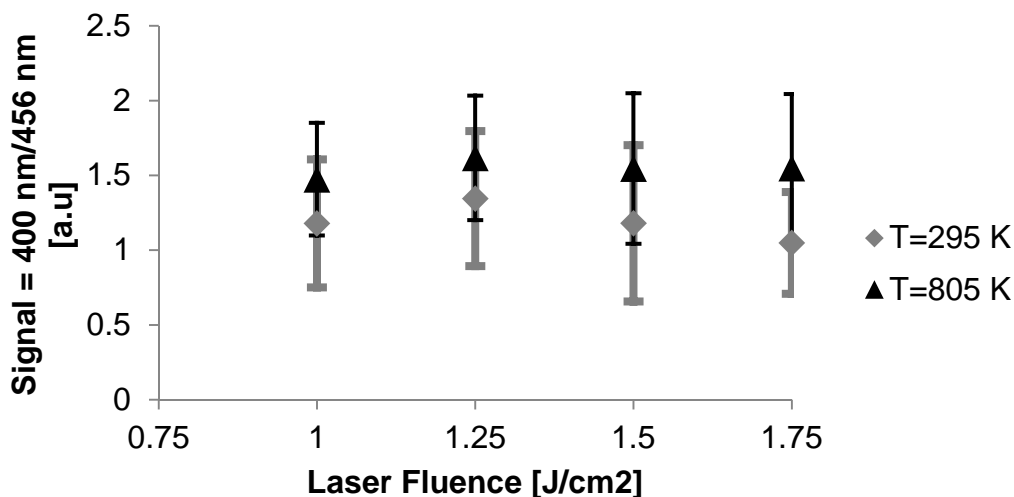

Figure 7: The spectral ratio of baked BAM particles at 295 K and 805 K as a function of laser fluence. The error bars represent one standard deviation of the individual particle ratios.

The average spectral ratios for unbaked BAM particles as a function of laser fluence are shown in Figure 8. Within the uncertainty of the measurements, the results indicate that $R_{295\,K}$ and $R_{805\,K}$ are independent of laser fluence from 0.3 to 0.9 J/cm^2. The average values of $R_{295\,K}$ and $R_{805\,K}$ are very similar at the two largest laser fluences. At the lowest laser fluence, the average value of $R_{805\,K}$ is greater than that of $R_{295\,K}$, but the difference only corresponds to one standard deviation. Overall, there does not appear to be a distinct dependence of the signal ratios on air temperature using the unbaked BAM particles. Therefore, the lack of temperature sensitivity in the spectral ratio of Fig. 7 cannot conclusively be attributed to degradation effects from baking. Spatial non-uniformities caused by the imaging optical components may be contribute to the observed temperature insensitivity. Fond *et al.* [11] reported that the spectral transmission profiles of their interference filters broadened slightly toward the UV as a function of incident angle and resulted in variations in the spectral transmission profile over the field of view. A spectrally independent and Lambertian light source is required for performing a flat-field correction and should account for these non-uniformities.
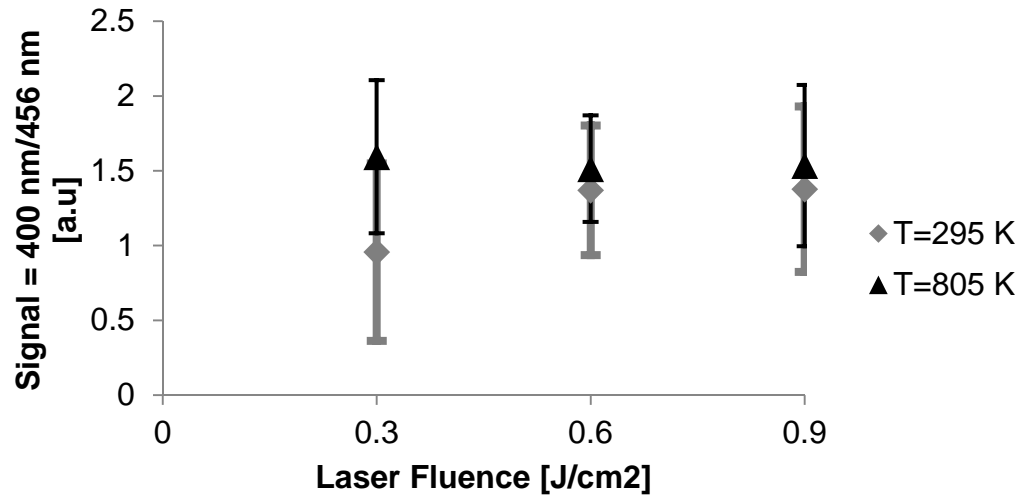
Figure 8: The spectral ratio of unbaked BAM particles at 295 K and 805 K as a function of laser fluence. The error bars represent one standard deviation of the individual particle ratios. Ratios at both temperatures are independent of laser fluence. Ratios within one standard deviation at 295 K and 805 K overlap and therefore do not indicate a distinct difference in air temperature.

5 CONCLUSIONS AND FUTURE WORK

Spectral ratio measurements on BAM particles were performed in a heated air flow at 295 K and 805 K for a range of laser fluences. Baked BAM particles were studied using laser fluences from $1 – 1.75$ J/cm^2. Unbaked BAM particles were studied using laser fluences from $0.3 – 0.9$ J/cm^2. An algorithm was developed to identify individual particles, match particle images with their corresponding image pair, and determine the spectral ratio for individual particles. The average spectral ratio for both baked and unbaked BAM particles was independent of the laser fluence. For both baked and unbaked particles, average spectral ratios within one standard deviation at 295 K and 805 K overlapped and therefore did not indicate a distinct difference in air temperature. The observed temperature insensitivity in the spectral ratio cannot be conclusively attributed to degradation from long baking times since unbaked phosphors also exhibited the same behavior. Further investigation is required to determine the cause of the spectral ratio's temperature insensitivity. The next step would be to measure the temperature dependence of the BAM phosphorescence emission spectra to verify the previously published results.

An additional improvement to the current set-up would be to use BAM phosphor particles that are coated with SiO_2 to reduce the likelihood of particle agglomeration. The coatings are on the order of several nanometers in thickness and therefore have a negligible impact on the particle size and the particle's flow tracing abilities. Lindén *et al*. [10] found that the spectral ratios of SiO_2 coated BAM particles do not differ from the ratios of uncoated BAM.

After issues with the phosphor's temperature sensitivity are resolved, the next step is to perform simultaneous stereo – PIV and temperature measurements using the single-camera lens assembly. Modification of previously developed PTV processing routines will be required to expand to full volumetric measurements. Finally, demonstration of full-3D capability should be conducted in heated flows and jet flames before ultimately applying the new tool to a motored engine.

REFERENCES

[1]   Lumley J. L., 1999, Engines: an introduction, Cambridge University Press, Cambridge ; New York.

[2]   Most D., and Leipertz A., 2001, "Simultaneous Two-Dimensional Flow Velocity and Gas Temperature Measurements by use of a Combined Particle Image Velocimetry and Filtered Rayleigh Scattering Technique," Applied Optics, **40**(30), p. 5379, doi:10.1364/AO.40.005379.

[3]   Peterson B., Baum E., Böhm B., Sick V., and Dreizler A., 2013, "High-speed PIV and LIF imaging of temperature stratification in an internal combustion engine," Proceedings of the Combustion Institute, **34**(2), pp. 3653–3660, doi:10.1016/j.proci.2012.05.051.

[4]   Omrane A., Petersson P., Aldén M., and Linne M. A., 2008, "Simultaneous 2D flow velocity and gas temperature measurements using thermographic phosphors," Applied Physics B, **92**(1), pp. 99–102, doi:10.1007/s00340-008-3051-1.

[5]   Someya S., Li Y., Ishii K., and Okamoto K., 2010, "Combined two-dimensional velocity and temperature measurements of natural convection using a high-speed camera and temperature-sensitive particles," Experiments in Fluids, **50**(1), pp. 65–73, doi:10.1007/s00348-010-0894-0.

[6]   Allison S. W., and Gillies G. T., 1997, "Remote thermometry with thermographic phosphors: Instrumentation and applications," Review of Scientific Instruments, **68**(7), p. 2615, doi:10.1063/1.1148174.

[7]   Khalid A. H., and Kontis K., 2008, "Thermographic Phosphors for High Temperature Measurements: Principles, Current State of the Art and Recent Applications," Sensors, **8**(9), pp. 5673–5744, doi:10.3390/s8095673.

[8]   Aldén M., Omrane A., Richter M., and Särner G., 2011, "Thermographic phosphors for thermometry: A survey of combustion applications," Progress in Energy and Combustion Science, **37**(4), pp. 422–461, doi:10.1016/j.pecs.2010.07.001.

[9]   Peterson K., Regaard B., Heinemann S., and Sick V., 2012, "Single-camera, three-dimensional particle tracking velocimetry," Optics Express, **20**(8), pp. 9031–9037, doi:10.1364/OE.20.009031.

[10]   Lindén J., Takada N., Johansson B., Richter M., and Aldén M., 2009, "Investigation of potential laser-induced heating effects when using thermographic phosphors for gas-phase thermometry," Applied Physics B, **96**(2-3), pp. 237–240, doi:10.1007/s00340-009-3608-7.

[11]   Fond B., Abram C., Heyes A. L., Kempf A. M., and Beyrau F., 2012, "Simultaneous temperature, mixture fraction and velocity imaging in turbulent flows using thermographic

phosphor tracer particles," Opt. Express, **20**(20), pp. 22118–22133, doi:10.1364/OE.20.022118.

[12]   Meng H., Pan G., Pu Y., and Woodward S. H., 2004, "Holographic particle image velocimetry: from film to digital recording," Measurement Science and Technology, **15**(4), pp. 673–685, doi:10.1088/0957-0233/15/4/009.

[13]   Pereira F., and Gharib M., 2002, "Defocusing digital particle image velocimetry and the three-dimensional characterization of two-phase flows," Measurement Science and Technology, **13**(5), pp. 683–694, doi:10.1088/0957-0233/13/5/305.

[14]   Brücker C., 1997, "3D scanning PIV applied to an air flow in a motored engine using digital high-speed video," Measurement Science and Technology, **8**(12), pp. 1480–1492, doi:10.1088/0957-0233/8/12/011.

[15]   2006, "Tomographic particle image velocimetry," Experiments in Fluids.

[16]   Arroyo M. P., and Greated C. A., 1991, "Stereoscopic particle image velocimetry," Measurement Science and Technology, **2**(12), pp. 1181–1186.

[17]   Fuhrmann N., Brübach J., and Dreizler A., 2013, "Phosphor thermometry: A comparison of the luminescence lifetime and the intensity ratio approach," Proceedings of the Combustion Institute, **34**(2), pp. 3611–3618, doi:10.1016/j.proci.2012.06.084.

[18]   Fuhrmann N., Schild M., Bensing D., Kaiser S. a., Schulz C., Brübach J., and Dreizler a., 2011, "Two-dimensional cycle-resolved exhaust valve temperature measurements in an optically accessible internal combustion engine using thermographic phosphors," Applied Physics B, **106**(4), pp. 945–951, doi:10.1007/s00340-011-4819-2.

[19]   Euler M., Kissel T., Dreizler A., and Brübach J., 2011, "The spectrally resolved luminescence decay of thermographic phosphors," Measurement Science and Technology, **22**(8), p. 083001, doi:10.1088/0957-0233/22/8/083001.

[20]   Wal R. L. V., Householder P. A., and Wright T. W., 1999, "Phosphor thermometry in combustion applications," Applied spectroscopy, **53**(10), pp. 1251–1258.

[21]   Särner G., Richter M., and Aldén M., 2008, "Investigations of blue emitting phosphors for thermometry," Measurement Science and Technology, **19**(12), p. 125304, doi:10.1088/0957-0233/19/12/125304.

[22]   Alharbi A. Y., 2010, "High-speed high-resolution vector field measurements and analysis of boundary layer flows in an internal combustion engine," University of Michigan.

[23]   Jainski C., Lu L., Dreizler A., and Sick V., 2012, "High-Speed Micro Particle Image Velocimetry Studies of Boundary-Layer Flows in a Direct-Injection Engine," International Journal of Engine Research, doi:10.1177/1468087412455746.

[24]   Incropera F. P., DeWitt D. P., Bergman T. L., and Lavine A. S., 2007, Fundamentals of heat and mass transfer, John Wiley, Hoboken.

[25]   Turos-Matysiak R., Grinberg M., Wang J. W., Yen W. M., and Meltzer R. S., 2007, "Luminescence of BAM under high pressure: the Eu2+ sites," Journal of Luminescence, **122-123**(0), pp. 107–109, doi:10.1016/j.jlumin.2006.01.111.

[26]   Bizarri G., and Moine B., 2005, "On phosphor degradation mechanism: thermal treatment effects," Journal of Luminescence, **113**(3-4), pp. 199–213, doi:10.1016/j.jlumin.2004.09.119.

[27]   Wang Y. H., and Zhang Z. H., 2005, "Luminescence Thermal Degradation Mechanism in BaMgAl[sub 10]O[sub 17]:Eu[sup 2+] Phosphor," Electrochemical and Solid-State Letters, **8**(11), p. H97, doi:10.1149/1.2063249.

[28]   Cosadia I., Borée J., Charnay G., and Dumont P., 2006, "Cyclic variations of the swirling flow in a Diesel transparent engine," Experiments in Fluids, **41**(1), pp. 115–134, doi:10.1007/s00348-006-0163-4.

[29]   White F. M., 2008, Fluid mechanics, McGraw-Hill, New York.

[30]   Konopliv N., and Sparrow E. M., "Transient heat conduction in non-homogeneous spherical systems," Heat and Mass Transfer, **3**(4), pp. 197–210, doi:10.1007/BF01106717.

[31]   Klein P. H., and Croft W. J., 1967, "Thermal Conductivity, Diffusivity, and Expansion of Y2O3, Y3 Al5O12, and LaF3 in the Range 77°–300°K," Journal of Applied Physics, **38**(4), p. 1603, doi:10.1063/1.1709730.

[32]   Versluis M., 2013, "High-speed imaging in fluids," Experiments in Fluids, **54**(2), p. 1458, doi:10.1007/s00348-013-1458-x.

[33]   Williams T. C., and Shaddix C. R., 2007, "Simultaneous correction of flat field and nonlinearity response of intensified charge-coupled devices.," The Review of scientific instruments, **78**(12), p. 123702, doi:10.1063/1.2821616.

[34]   Lipzig J. P. J., Yu M., Dam N. J., Luijten C. C. M., and Goey L. P. H., 2013, "Gas-phase thermometry in a high-pressure cell using BaMgAl10O17:Eu as a thermographic phosphor," Applied Physics B, doi:10.1007/s00340-013-5360-2.

Distribution

| 1 | MS0899 | Technical Library | 9536 (electronic copy) |

For LDRD reports, add:

| 1 | MS0359 | D. Chavez, LDRD Office | 1911 |